

Alma Mater Studiorum Università di Bologna  
Archivio istituzionale della ricerca

Off-rift volcanism in rift zones determined by crustal unloading

This is the final peer-reviewed author's accepted manuscript (postprint) of the following publication:

*Published Version:*

Maccaferri, F., Rivalta, E., Keir, D., Acocella, V. (2014). Off-rift volcanism in rift zones determined by crustal unloading. NATURE GEOSCIENCE, 7(4), 297-300 [10.1038/ngeo2110].

*Availability:*

This version is available at: <https://hdl.handle.net/11585/775989> since: 2020-10-25

*Published:*

DOI: <http://doi.org/10.1038/ngeo2110>

*Terms of use:*

Some rights reserved. The terms and conditions for the reuse of this version of the manuscript are specified in the publishing policy. For all terms of use and more information see the publisher's website.

This item was downloaded from IRIS Università di Bologna (<https://cris.unibo.it/>).  
When citing, please refer to the published version.

(Article begins on next page)

This is the final peer-reviewed accepted manuscript of:

Maccaferri, F., Rivalta, E., Keir, D. e Acocella, V. Off-rift volcanism in rift zones determined by crustal unloading. *Nature Geoscience* 7, 297–300 (2014).

The final published version is available online at: <https://doi.org/10.1038/ngeo2110>

#### Rights / License:

The terms and conditions for the reuse of this version of the manuscript are specified in the publishing policy. For all terms of use and more information see the publisher's website.

*This item was downloaded from IRIS Università di Bologna (<https://cris.unibo.it/>)*

***When citing, please refer to the published version.***

# Unloading-driven off-rift distribution of volcanism in rift zones

Francesco Maccaferri<sup>1,2\*</sup>, Eleonora Rivalta<sup>1,2</sup>, Derek Keir<sup>3</sup>, Valerio Acocella<sup>4</sup>

1 GeoForschungsZentrum Potsdam, Section 2.1, Helmholtzstrasse 7, 14467, Potsdam, Germany

2 Institute of Geophysics, University of Hamburg, Bundesstr. 55, 20146, Hamburg, Germany;

3 National Oceanography Centre Southampton, University of Southampton, Southampton, SO14 3ZH, UK

4 Dipartimento Scienze, University of Roma Tre, L. S.L. Murialdo, 1, 00146, Roma, Italy.

\*Corresponding author. Email: [francesco.maccaferri@gfz-postdam.de](mailto:francesco.maccaferri@gfz-postdam.de)

**Prolonged extension of the continents results in deep elongated rift valleys at the surface and a rift-centred magma ponding zones at the crust-mantle boundary<sup>1,2</sup>. The ascending magma sometimes erupts to the surface producing volcanism both in the rift valley<sup>3,4</sup>, or counterintuitively, at off-rift volcanic fields offset by tens of kilometres from the source of magma at depth<sup>5,6,7,8</sup>. The driving forces behind the off-rift surface distribution of magmatism remain enigmatic. Here we demonstrate, with numerical models of dyke propagation, that the gravitational unloading induced by crustal thinning and rift border faulting can steer dykes away from the deep magma ponding zone towards the rift sides, eventually causing eruptions at tens of kilometres outside the rift border. Furthermore, our models predict the formation of stacked magmatic sills in the lower crust above the magma ponding zone, and the along-rift propagation of shallow dykes in rifting events. Gravitational unloading, which facilitates decompression melting of the asthenosphere, is fundamental in controlling the transfer of magma from depth to the surface. Our predictions are consistent with the location and shape of intrusions, as well as the distribution of volcanism from rift zones around the Earth.**

Continental rifts are commonly flanked by magmatism during their early stages<sup>5,6</sup>. In the Miocene-Recent Main Ethiopian Rift (MER), for example, many Pliocene volcanoes lie outboard of the Miocene rift border faults<sup>9,10</sup> (Fig. 1). As the cumulative extension has increased, magmatism has become

31 focused within the rift axis<sup>3</sup>. A similar pattern is observed during the evolution of the Red Sea Rift,  
32 where ~25 Ma-old rift-parallel dykes focus near the ~30 Ma-old rift margins, and the youngest  
33 volcanoes focus along the ridge axis<sup>11</sup>. Even in far less magmatically active settings, such as the Baikal  
34 Rift (Siberia) or the Chaîne des Puys (CdP) in the Cenozoic rift system of France, off-rift volcanism  
35 occurred after the onset of rifting<sup>7,8</sup>.

36 During rift initiation, the lithosphere thins by ductile stretching beneath a rift valley formed from  
37 normal faulting<sup>12</sup>. The upwelling asthenosphere melts by adiabatic decompression, with the greatest  
38 degree of partial melting beneath the most thinned rift valley<sup>1,2</sup>. While most studies focus on in-rift  
39 magmatism<sup>3,4</sup>, a model is needed to explain how off-rift volcanoes are fed. Progressive rift spreading  
40 results in the oldest volcanoes being transported away from the rift axis. However, such a process does  
41 not explain off-rift volcanism, with volcanoes located outside the rift border faults. Previous models for  
42 off-rift volcanoes include low-angle detachments tapping the asthenosphere to the sides of highly  
43 asymmetric rifts<sup>13</sup>, or the flexural response at the base of the footwall of the active rift border faults<sup>5</sup>.  
44 These models are unsatisfactory, because geophysical evidence of highly asymmetric magmatic rifts  
45 and offset magmatic sources is lacking, and any flexural response should induce horizontal  
46 compression at the top of the footwall of the rift border faults, preventing shallow dyke propagation.

47

48 While magma at mantle depths ascends by porous flow, in the crust dyking is the most viable  
49 mechanism of transport. We use numerical models to investigate the ascent of magma-filled dykes in  
50 the stress field induced in the elastic layers of the crust by tectonic extension and unloading due to a  
51 topographic depression<sup>14</sup>. Elastic shear stresses in the upper crust are expected to persist over millions  
52 of years; the effect of a weak lower crust is discussed below. With a 2D numerical model<sup>15</sup> we calculate  
53 the trajectories of ascending dykes from a magma ponding zone at the crust-mantle boundary or from a  
54 crustal reservoir (at depth  $z_{in}$ ) with lateral extent equal to the half width of the graben (Fig. 2). We  
55 model dykes as boundary-element cracks composed of  $N$  contiguous and interacting dislocation  
56 elements propagating in a brittle elastic half-space. The dyke opens under assigned normal and shear  
57 stress given by the internal overpressure and by the shear component of the tectonic plus unloading  
58 stresses, respectively. The overpressure within the dyke is the difference between the magma pressure  
59 and the confining stress: which is the superposition of the lithostatic pressure, the normal component of  
60 the topographic unloading and the tectonic stress (assumed as homogeneous horizontal stretching  $\sigma_{tec}=5$

61 MPa). The fluid pressure is given by a magma-static (linear) profile and accounts for magma  
 62 compressibility, with a magma-rock density contrast of 80-300 kg m<sup>-3</sup> (Table S1). The dykes are  
 63 nucleated perpendicular to the minimum compressive stress  $\sigma_3$ . Their trajectories are calculated by  
 64 testing incremental elongations in different directions and selecting the one maximizing the elastic and  
 65 gravitational energy release<sup>15</sup>.

66

67 Our models suggest that dykes may reach the surface both within and outside the rift, depending on the  
 68 competition between tectonic stretching and unloading pressure, and on the nucleation depth of the  
 69 dykes. The unloading stress field is controlled by the graben width,  $W$ , and the effective depth,  $D$ ,  
 70 accounting for the total deficit of mass from the topographic depression and low-density sediments.  
 71 When the unloading pressure  $P_0 = \rho g D$  ( $\rho$  is crustal density,  $g$  acceleration due to gravity) dominates  
 72 over the tectonic stretching ( $K = \pi \sigma_{tec} / (2P_0) < 1$ , which translates into  $D > \pi \sigma_{tec} / (2\rho g) \sim 250$  m for  $\rho = 3000$  kg  
 73 m<sup>-3</sup>, see Method Summary),  $\sigma_3$  becomes vertical beneath the rift in a volume centred at a depth  
 74  $z_c = \rho g D W / (\pi \sigma_{tec})$  with upper and lower depths  $z_1 = (W/2K)[1 - (1-K^2)^{1/2}]$  and  $z_2 = (W/2K)[1 + (1-K^2)^{1/2}]$ ,  
 75 respectively (Methods; Fig. 3c). This volume constitutes a stress barrier zone that deflects the  
 76 ascending dykes to the rift sides. Sideways from the rift centre,  $\sigma_3$  becomes first inward dipping and  
 77 then horizontal (Fig. 3). A similar pattern for  $\sigma_3$ , on a smaller scale, was obtained by modelling the  
 78 unloading due to ice-cap retreat at Kverkfjöll volcano, Iceland<sup>16</sup>.

79 Depending on where the dykes nucleate relative to the stress barrier zone, three scenarios for their  
 80 propagation and for the final surface distribution of magmatism occur:

81 1) When  $z_{in} < z_1$  in-rift volcanism occurs. Magma-filled dykes ascend subvertically, or propagate laterally  
 82 within the rift parallel to the axis (Fig. 3a). The dyke arrivals are spread within the graben (vertical bars  
 83 in Fig. 4a for  $x^* < 1$ ). For deep grabens  $z_1$  is shallow ( $D \sim 1$  km and  $W \sim 100$  km gives  $z_1 \sim 10$  km) so that  
 84 in-rift arrivals occur only for shallow nucleation depths. For a nucleation depth of 40 km, in-rift  
 85 volcanism occurs only for wide ( $> 100$  km) and shallow ( $< 0.6$  km) rift depressions, for which the  
 86 ponding zone is above the stress barrier, or the graben depth is too small to create one ("in-rift  
 87 volcanism" area in Fig. 4b). Shallower nucleation depths result in enlarging the "in-rift volcanism" area  
 88 (Fig. 4c), as expected for the North Volcanic Zone of Iceland (NVZ) and for Quaternary volcanism in  
 89 the MER.

90 2) When  $z_1 < z_{in} < z_2$ , our model predicts off-rift volcanism with sill formation. The injected magma forms

91 sub-horizontal magmatic sheets that, depending on their initial distance from the rift axis, get trapped  
 92 as stacked sills above the ponding zone or escape to the side of the stress barrier, turning into  
 93 subvertical dykes and eventually reaching the surface (Fig. 3b). The dyke arrival distance as a function  
 94 of  $z_{in}$  scales with the rift width (Fig. 4a). For a given set of parameters, dykes emerge very tightly  
 95 spaced at a distance from the rift axis equal to about 1 to 2 (and up to 3) graben half-widths (Fig. 4a,  
 96  $x^* > 1$ ). This may result in the construction of large off-rift volcanoes aligned parallel to the rift. As the  
 97 rift matures, the magma ponding zone near the base of the crust becomes progressively shallower due  
 98 to crustal thinning and to sills piling one above the other and functioning as new, shallower reservoirs,  
 99 driving the system towards the condition of case 1 and to a transition to in-rift volcanism (Fig. 4c).

100 3) When  $z_{in} > z_2$ , off-rift volcanism occurs without sill formation: vertical dykes are deflected towards  
 101 the rift sides, with a more scattered arrival distribution at the surface (Fig 3c).  $z_2$  being relatively deep,  
 102 this occurs with deep nucleation depths below shallow and narrow grabens, as illustrated by the three  
 103 points in the dashed rectangle in Fig. 4a, and the case  $W=25$  km,  $D=0.4$  km in Fig. 4b.

104

105 The stress barrier is only maintained in the elastic layer. Observations of deep seismicity in young rifts  
 106 suggest a strong mid-lower crust<sup>17,18,19</sup> that maintains the stresses necessary to create a stress barrier at  
 107 any crustal depth. If the lower crust and upper mantle are weak, the elastic stresses dissipate, and  $z_2$   
 108 may coincide with the bottom of the elastic layer.

109

110 For a given nucleation depth, the aspect ratio of the rift depression determines in-rift or off-rift dyke  
 111 propagation. Shallow and wide rift depressions favour in-rift dyke arrivals, whereas narrow and deep  
 112 depressions favour off-rift arrivals, coupled or not with sill intrusions at depth (Fig. 4b). The relative  
 113 proportion of extruded to intruded magma decreases for deep and narrow grabens, approaching non-  
 114 volcanic rifts (Fig. 4b, “only sill formation” area). In general, this also depends strongly on model  
 115 parameters such as magma buoyancy, initial volume of the magma batches (controlling the dyke  
 116 driving pressure) and crustal fracture toughness. For example, the “only sill formation” area of Fig. 4b  
 117 disappears if magma buoyancy is increased by 15% (Table 1, supplementary material), or if the initial  
 118 volume is doubled. Also, the scarcity of sills in Fig. 4c is due to a higher magma buoyancy linked to a  
 119 lower initial confining pressure. The dyke driving pressure does not impact significantly on  $x_{dr}$ , as with  
 120 our parameters the unloading stresses dominate over dyke driving pressure.

121 Our model is consistent with observations from major rift systems. For parameters appropriate for the  
122 MER, CdP and Baikal rifts, we expect sill stacking and off-rift volcanism. Indeed, in these cases the  
123 lower crust is heavily intruded with sills<sup>20,21</sup>, and off-rift volcanism has accompanied early rifting<sup>5,7</sup>  
124 (Fig. 1 and Table S2 for numerical values of  $W$  and  $D$ ). At the MER, the off-rift volcanic rocks have  
125 experienced fractional crystallisation pressure higher than the volcanism found along the rift axis, sug-  
126 gesting that magma feeding off-rift volcanoes stalls at greater crustal depths than those in the rift axis,  
127 likely because of their more complex pathway. However, both magmas originate from the same parent-  
128 al source of basalts formed from decompressional melting of the upper asthenosphere beneath the  
129 rift<sup>22,23</sup>. The basalts exhibit differences in major and trace elements, and radiogenic isotopes that vary  
130 more over the distances of adjacent scoria cones than between the axial and flank volcanic fields<sup>24</sup>.

131 Importantly, as the crust thins and sills progressively stack, causing the shallowing of the injection  
132 depth, eventually up to  $z=z_1$ , where  $\sigma_3$  turns horizontal, the magma pathways and volcanism become  
133 confined to the rift centre. In more evolved rifts where protracted intrusion has significantly heated the  
134 plate, such as in Afar, <10 km-deep magma reservoirs beneath axial volcanoes are common<sup>25,26</sup> and  
135 feed episodic dykes along the axis<sup>4,27</sup>.

136 Our model is also consistent with observations of subvertical dykes feeding off-rift volcanism and ~20-  
137 25 Ma basaltic dyke swarms along the Red Sea rift margin<sup>28</sup>, that are thought to accommodate strain  
138 after the onset of rifting at 29-31 Ma<sup>11,29</sup>. In contrast, rifts with mild topographic expression (wide and  
139 shallow depression), such as the NVZ, lack significant off-rift volcanism. This is predicted by our  
140 model, since the very shallow injection depth, which is above the expected stress barrier zone, creates a  
141 wide dyke swarm area within the rift (Fig. 3a).

142  
143 Earlier models considered flexure of the lithosphere and interaction of magma with large boundary  
144 faults to explain rift flank volcanism<sup>5</sup>. Boundary faults certainly influence the ascent of magma in the  
145 upper crust. However, our models suggest that if unloading stresses are ignored, dykes from a ponding  
146 zone beneath the rift ascending in a stress field associated with normal faults, always reach the surface  
147 within the graben (Fig. S1, supplement). The flexural behaviour of the crust may add local variations in  
148 the stress pattern, not expected to alter the overall distribution of stresses<sup>5</sup>; in addition, the flexural  
149 response to rifting creates topography highs at the rift shoulders, attracting dykes and reinforcing off-

150 rift magmatism<sup>14,30</sup>.

151 Our model may shed light on the history of tectonically complicated areas, such as the Upper Rhine  
152 Graben and other fossil continental rifts in which the existence or non-existence of surface volcanism  
153 has remained unexplained.

154

155

## 156 **Method Summary**

157 Considering a plane ( $x, z$ ), perpendicular to the rift and with origin at the rift center (see Fig. 2) we  
158 express the condition for which  $\sigma_3$  is vertical along the  $z$  axis (vertical, downward directed) by requiring  
159 that:

$$160 \sigma_{zz}(x=0, z) > \sigma_{xx}(x=0, z) + \sigma_{tec} \quad (1)$$

161 being the unloading shear stresses null in  $x=0$ . By calculating  $\sigma_{zz}$  and  $\sigma_{xx}$  from the formulas for the  
162 unloading<sup>14, 30</sup>, we find that the stress barrier is located at depth:

$$163 \frac{W}{2} \cdot \frac{1 - \sqrt{1 - K^2}}{K} < z < \frac{W}{2} \cdot \frac{1 + \sqrt{1 - K^2}}{K} \text{ if } K = \frac{\pi}{2} \cdot \frac{\sigma_{tec}}{P_0} < 1 \quad (2)$$

164 If  $K > 1$  (equivalent to  $D < \pi \sigma_{tec} / (2\rho g)$ ), eq. (1) does not hold for any  $z$  and vertical dyke propagation will  
165 always be favoured.  $\sigma_t$  is always perpendicular to the page in  $x=0$  in our plain strain approximation  
166 model ( $\sigma_{yy} = \nu(\sigma_{xx} + \sigma_{zz})$ , with  $\nu$  Poisson's number).

167 Eq. (2) can be non-dimensionalised by using  $z^* = z / (W/2)$ :

$$168 \frac{1 - \sqrt{1 - K^2}}{K} < z^* < \frac{1 + \sqrt{1 - K^2}}{K}$$

169 The non-dimensional centre of the stress barrier is  $c^* = K^{-1}$  and its extension is  $e^* = (2/K)(1 - K)^{1/2}$ .

170

## 171 **References:**

172

- 173 1. Lubimova, E. A. Heat flow patterns from Baikal and other rift zones. *Tectonophysics* **8**, 457-467  
174 (1969).
- 175 2. Bown, J. W. & White, R. S. Effect of finite extension rate on melt generation at rifted continental  
176 margins. *J. Geophys. Res.* **100**, 18011-18029 (1995).
- 177 3. Ebinger, C. J. & Casey, M. Continental breakup in magmatic provinces: an Ethiopian example.



178      *Geology* **29**, 527-530 (2001).

179    4. Wright, T. J. *et al.* Magma maintained rift segmentation at continental rupture in the 2005 Afar  
180      dyking episode. *Nature* **442**, 291-294 (2006).

181    5. Ellis, M. & King, G. Structural control of flank volcanism in continental rifts. *Science* **254**, 839-842  
182      (1991).

183    6. Morton, W. H., Mitchell, J. G., Rex, D. C. & Mohr, P. Riftward younging of volcanic units in the  
184      Addis-Ababa region, Ethiopian rift valley. *Nature* **280**, 284-288 (1979).

185    7. Kiselev, A. I. Volcanism of the Baikal rift zone. *Tectonophysics* **143**, 235-244 (1987).

186    8. Richet, P. *Guide des Volcans de France*. (BRGM Belin, Paris, 2003).

187    9. Abebe, T., Mazzarini, F., Innocenti, F. & Manetti, P. The Yerer-Tullu Wellel volcanotectonic  
188      lineament: a transitional structure in central Ethiopia and the associated magmatic activity. *J.*  
189      *African Earth Sci.* **26**, 135-150 (1998).

190    10. Chernet, T., Hart, W. K., Aronson, J. L. & Walter, R. C. New age constraints on the timing of  
191      volcanism and tectonism in the northern Main Ethiopian Rift – southern Afar transition zone  
192      (Ethiopia). *J. Volcanol. Geotherm. Res.* **80**, 267-280 (1998).

193    11. Bosworth, W., Huchon, P. & McClay, K. The Red Sea and Gulf of Aden Basins. *J. African Earth*  
194      *Sci.* **43**, 334-378 (2005).

195    12. McKenzie, D. Some remarks on the development of sedimentary basins. *Earth Planet. Sci. Lett.* **40**,  
196      25-32 (1978).

197    13. Bosworth, W. Off-axis volcanism in the Gregory rift, east Africa: implications for models of  
198      continental rifting. *Geology* **15**, 397-400 (1987).

199    14. Davis, R. & Selvadurai, A. *Elasticity and Geomechanics* (Cambridge Univ. Press, Cambridge,  
200      1996).

201    15. Maccaferri, F., Bonafede, M. & Rivalta, E. A quantitative study of the mechanisms governing dike  
202      propagation, dike arrest and sill formation. *J. Volcanol. Geotherm. Res.* **208**, 39-50 (2011).

203    16. Hooper, A. *et al.* Increased capture of magma in the crust promoted by ice-cap retreat in Iceland.  
204      *Nature Geoscience* **4**, 783-786 (2011).

205    17. Deverchere, J. *et al.*, Depth distribution of earthquakes in the Baikal rift system and its implications  
206      for the rheology of the lithosphere, *Geophys. J. Int.* **146**, 714-730 (2001).

207    18. Foster, A.N., and Jackson, C.A., Source parameters of large African earthquakes: implications for

- 208 crustal rheology and regional kinematics, *Geophys. J. Int.* **134**, 422-448 (1998).
- 209 19. Craig, T.J., Jackson, C.A., Preistley, K., McKenzie, D., Earthquake distribution patterns in Africa:  
210 their relationship to variations in lithospheric and geological structure, and their rheological  
211 implications, *Geophys. J. Int.* **185**, 403-434 (2011).
- 212 20. Thybo, H. & Nielsen, C. A. Magma-compensated crustal thinning in continental rift zones. *Nature*.  
213 **457**, 873-876 (2009).
- 214 21. Mackenzie, G. D., Thybo, H. & Maguire, P. K. H. Crustal velocity structure across the Main  
215 Ethiopian rift: Results from 2-dimensional wide-angle seismic modeling. *Geophys. J. Int.* **162**, 994-  
216 1006 (2005).
- 217 22. Peccerillo, A. *et al.* Petrogenesis of silicic peralkaline rocks in the Ethiopian Rift: geochemical  
218 evidence and volcanological implications. *J. African Earth Sci.*, **48**, 161-173 (2007).
- 219 23. Rooney, T.O., Furman, T., Bastow, I., Ayalew, D., Yirgu, G., Lithospheric modification during  
220 crustal extension in the Main Ethiopian rift, *J. Geophys. Res.* **112**, B10201 (2007).
- 221 24. Rooney, T.O., Bastow, I.D., Keir, D., Insights into extensional processes during magma assisted  
222 rifting: Evidence from aligned scoria cones, *J. Volcanol. Geotherm. Res.* **201**, 83-96, (2011).
- 223 25. Pagli, C. *et al.* Shallow axial magma chamber at the slow-spreading Erta Ale Ridge. *Nature*  
224 *Geoscience* **5**, 284-288 (2012).
- 225 26. Nobile, A. *et al.* Dike-fault interaction during the 2004 Dallol intrusion at the northern edge of the  
226 Erta Ale Ridge (Afar, Ethiopia). *Geophys. Res. Lett.* **39**, L19305 (2012).
- 227 27. Grandin, R. *et al.* Seismicity during lateral dike propagation: Insights from new data in the recent  
228 Manda Hararo-Dabbahu rifting episode (Afar, Ethiopia). *Geochem. Geophys. Geosyst.* **12**, Q0AB08  
229 (2011).
- 230 28. Pallister, J. S. *et al.* Broad accommodation of rift-related extension recorded by dyke intrusion in  
231 Saudi Arabia. *Nature Geoscience* **3**, 703-710 (2010).
- 232 29. Wolfenden, E., Ebinger, C. J., Yirgu, G., Renne, P. & Kelley, S. P. Evolution of a volcanic rifted  
233 margin: Southern Red Sea, Ethiopia. *Geol. Soc. Am. Bull.* **117**, 846-864 (2005).
- 234 30. Dahm, T. Numerical simulations of the propagation path and the arrest of fluid-filled fractures in  
235 the Earth. *Geophys. J. Int.* **141**, 623-638 (2000).
- 236
- 237

238 **Corresponding author**

239 Correspondence and requests for materials should be addressed to Francesco Maccaferri. Email:  
240 francesco.maccaferri@gfz-potsdam.de

241

242 **Acknowledgements**

243 Carolina Pagli is acknowledged for extracting the SRTM DEM for the Chaîne de Puys. Comments  
244 from three anonymous reviewers improved the work. The work was funded by the ERC StG project N.  
245 240583 CCMP-POMPEI. VA acknowledges PRIN 2009 project.

246

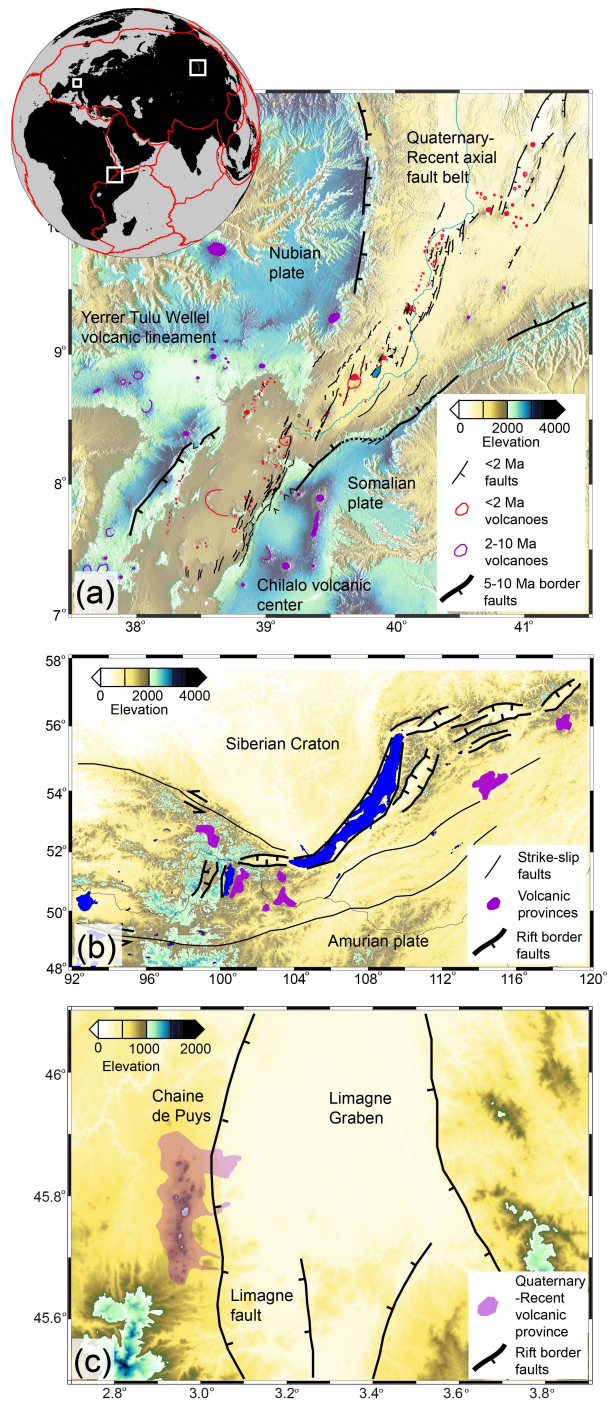
247 **Author Contributions**

248 FM and ER planned the paper, the numerical experiments and formulated the analytical modelling. FM  
249 implemented and run the BE code. DK and VA compared the numerical results with natural cases. DK  
250 made Fig. 1 with input from VA. FM made Fig. 2, 3 and 4 with input from ER. All authors discussed  
251 the results and contributed in writing the manuscript.

252

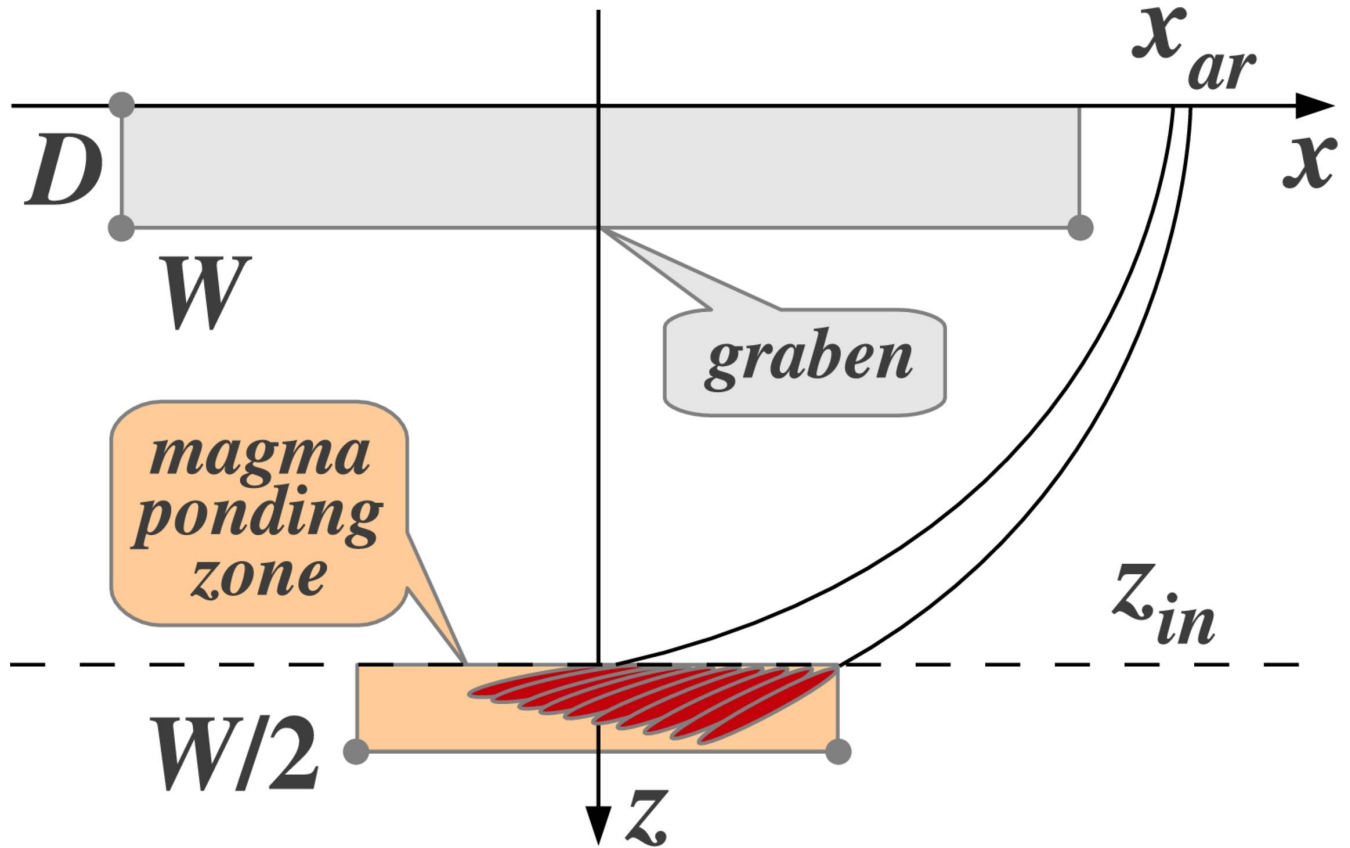
253 **Figures:**

254

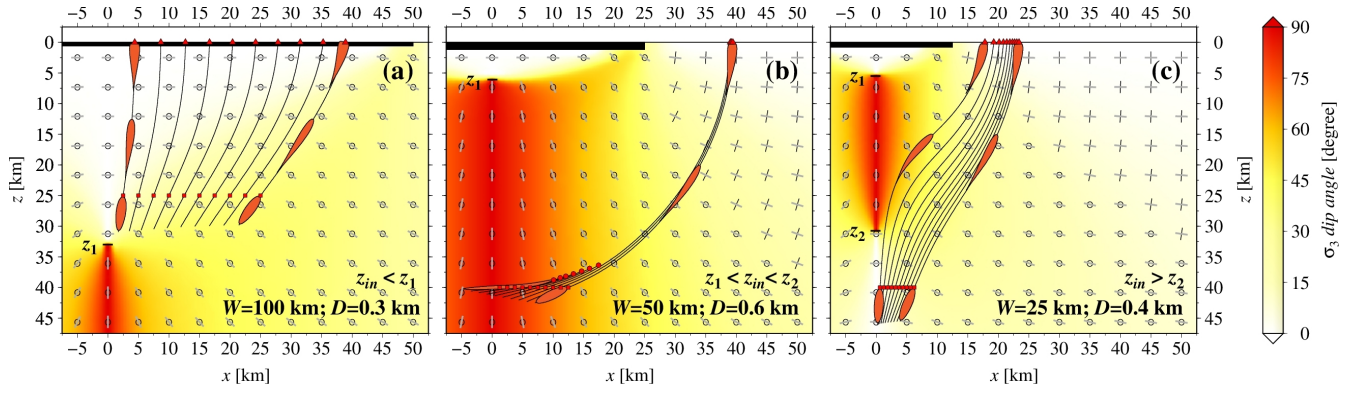


256 **Figure 1: Topographic, structural and volcanic architecture of the Main Ethiopian Rift (a),**  
 257 **Baikal Rift (b) and Chaîne de Puys (c).** For the MER, Miocene border faults are thick black lines  
 258 with direction of down throw indicated and the Quaternary-Recent faults within the rift are thin black

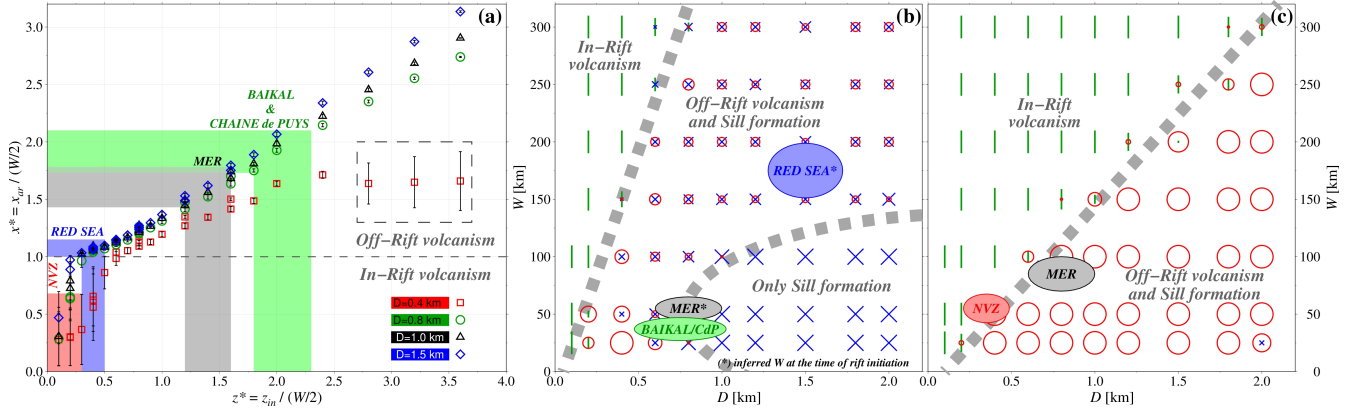
259 lines. Early syn-rift volcanic edifices are purple and Quaternary-Recent volcanoes and cones are red.  
 260 Note that the early syn-rift volcanism ranges from being just outboard of the Miocene border faults, to  
 261 as far as 100 km from the rift valley. For the Baikal Rift and Chaine de Puys major rift normal faults  
 262 are thick black lines and the spatial extent of volcanism is shown in purple.  
 263



265 **Figure 2: Set-up for the numerical experiments.** In each model ten equally spaced dykes are released  
 266 at  $z_{in}$  from half of a ponding zone as wide as half width of the graben. One simulation corresponds to a  
 267 run of each individual dyke. All the parameters employed in the numerical runs are listed in Table S1,  
 268 supplementary material.



270 **Figure 3: Dyke trajectories for  $z_{in}$  above (a), within (b) and below (c) the stress barrier zone.** Red  
 271 squares indicate the upper tip of the dyke at injection, red circles indicate that a dyke has been arrested  
 272 as sill; red triangles indicate the position of the arrival at surface. Black and gray segments show the  
 273 directions of  $\sigma_1$  and  $\sigma_3$  respectively (a circle indicates direction perpendicular to the page) for three  
 274 nominal sets of graben width,  $W$ , and depth,  $D$ , (see insets). The dip angle of  $\sigma_3$  is color-shaded: where  
 275 sub-vertical (reddish color), a stress barrier to vertical ascent of dykes is acting. The stress barrier is  
 276 expected to dissipate in a weak lower crust or mantle.



278 **Figure 4: Summary of the numerical results. a,** Normalized arrival distance  $x^*=x_{ar}/(W/2)$  from the  
 279 rift axis as a function of the normalized injection depth  $z^*=z_{in}/(W/2)$ . The vertical bars indicate the  
 280 spatial spreading of dyke arrivals at surface. The vertical shaded areas locate on the diagram four rift  
 281 systems. The dashed rectangle highlights 3 points for which  $z_{in} < z_2$ . **b,** Results for  $z_{in}=40$  km. The size  
 282 of the symbols (I, O and X) is proportional to the number of dykes that end up in-, off-rift or as sills  
 283 respectively. **c,** same as b, with  $z_{in}=20$  km.